Title
Ancestral roles of atypical cadherins in planar cell polarity

Journal
Proceedings of the National Academy of Sciences of the United States of America, 117(32)

ISSN
0027-8424

Authors
Brooun, Maria
Klimovich, Alexander
Bashkurov, Mikhail
et al.

Publication Date
2020-08-11

DOI
10.1073/pnas.1917570117

Peer reviewed

Ancestral roles of atypical cadherins in planar cell polarity

Maria Brooun[a,1], Alexander Klimovich[b], Mikhail Bashkurov[a], Bret J. Pearson[c,d,e], Robert E. Steele[f], and Helen McNeill[a,d,g,1]

[a]Lunenfeld-Tanenbaum Research Institute of Mount Sinai Hospital, Sinai Health System, Toronto, ON M5G 1X5, Canada; [b]Zoological Institute, Christian-Albrechts University of Kiel, 24118, Kiel, Germany; [c]Program in Developmental and Stem Cell Biology, The Hospital for Sick Children, Toronto, ON M5G 0A4, Canada; [d]Department of Molecular Genetics, University of Toronto, Toronto, ON M5S 1A8, Canada; [e]Ontario Institute for Cancer Research, MaRS Center, Toronto, ON M5G 0A3, Canada; [f]Department of Biological Chemistry, University of California, Irvine, CA 92697; and [g]Department of Developmental Biology, Washington University School of Medicine, St. Louis, MO 63110

Edited by Alejandro Sánchez Alvarado, HHMI, Stowers Institute for Medical Research, Kansas City, MO, and approved June 30, 2020 (received for review October 9, 2019)

Fat, Fat-like, and Dachsous family cadherins are giant proteins that regulate planar cell polarity (PCP) and cell adhesion in bilaterians. Their evolutionary origin can be traced back to prebilaterian species, but their ancestral function(s) are unknown. We identified Fat-like and Dachsous cadherins in *Hydra*, a member of phylum Cnidaria a sister group of bilaterian. We found *Hydra* does not possess a true Fat homolog, but has homologs of Fat-like (HyFatl) and Dachsous (HyDs) that localize at the apical membrane of ectodermal epithelial cells and are planar polarized perpendicular to the oral–aboral axis of the animal. Using a knockdown approach we found that HyFatl is involved in local cell alignment and cell–cell adhesion, and that reduction of HyFatl leads to defects in tissue organization in the body column. Overexpression and knockdown experiments indicate that the intracellular domain (ICD) of HyFatl affects actin organization through proline-rich repeats. Thus, planar polarization of Fat-like and Dachsous cadherins has ancient, prebilaterian origins, and Fat-like cadherins have ancient roles in cell adhesion, spindle orientation, and tissue organization.

Hydra | planar cell polarity | evolution | adhesion | cadherins

Planar cell polarity (PCP) is the coordinate polarization of cells within the plane of a tissue. PCP signaling regulates a wide range of tissue organization in animal development, from hairs on insect wings, to convergent extension movements during vertebrate gastrulation, and oriented cell divisions (1). The mechanisms controlling PCP were first deciphered in *Drosophila* and have been shown to be conserved in bilaterians. Several modules are known to regulate planar polarity. The most studied and best understood is the "core module," consisting of a number of transmembrane proteins and associated cytoplasmic components, such as Flamingo, Frizzled, Dishevelled, Strabismus, and Prickle (reviewed in ref. 1).

Another critical regulator of planar polarity is the Fat/Dachsous (Fat/Ds) complex, consisting of two giant atypical cadherins, Fat and Ds. Fat and Ds interact via extracellular cadherin domains, and use their intracellular domains to transduce planar polarity signals, as well as to control proliferation via the Hippo pathway and to mediate metabolic control (reviewed in refs. 2 and 3). In addition, a closely related family of Fat-like cadherins, similar in their extracellular domains but with a distinct intracellular domain, can planar polarize cells and influence actin and microtubule dynamics (4–8). Although the extracellular domains of Fat and Fat-like cadherins are similar, Ds binding has only been observed with the Fat/Fat4 family of cadherins.

Fundamental questions regarding the origin and ancestral functions of PCP genes remain unanswered. For example: How did PCP evolve, and what is the minimal machinery required to polarize a cell within tissues? Homologs of PCP proteins have been identified across the animal kingdom (9–12); however, only the core PCP protein Strabismus has been studied in nonbilaterians, where it is required for gastrulation in the cnidarians *Nematostella* and *Clytia* (13, 14). Core PCP proteins have also been identified in the cnidarian *Hydra* (15); however, the functions of Fat or Fat-like cadherins in cnidarians have not been explored.

The freshwater cnidarian polyp *Hydra* is radially symmetric and has only two cell layers, an ectoderm and an endoderm. Both layers are composed of epithelial cells with intermingled cells of the interstitial stem cell lineage (16). The *Hydra* body column is a cylinder, with a head at one (oral) end and a foot at the other (aboral) end (Fig. 1 *A* and *B*). The head contains the mouth and a ring of tentacles. Epithelial cells of the body column divide continuously and are constantly displaced toward the oral and aboral ends of the polyp, where they differentiate into head- and foot-specific cells and are eventually sloughed off (17). The orientation of cell divisions in the body column along the oral–aboral axis is thought to be a form of planar polarization (18). The direction of cell displacement changes when cells enter the tentacles and when a bud, *Hydra*'s asexual form of reproduction, is formed (Fig. 1 *A* and *B*) (19). Another planar polarized feature of the *Hydra* body column is the organization of basal contractile protrusions of epithelial cells, which are called myonemes. Myonemes are oriented along the oral–aboral axis in the ectoderm and circumferentially in the endoderm (Fig. 1*C*).

In *Hydra*, expression of the core PCP genes *frizzled* and *dishevelled* is strongly up-regulated at the bases of the tentacles and early in bud evagination (15), suggesting that the core PCP

Significance

Planar cell polarization, PCP, describes a form of organization where every cell within a group acquires the same planar characteristics, whether it is orientation of cell division, direction of migration, or localization of a cellular structure. PCP is essential for correct organization of cells into tissues and building a proper body plan. Here we use *Hydra*, an organism with a single axis of symmetry and a very simple body plan to investigate the function of the cell adhesion molecules Fat-like and Dachsous. We show that *Hydra* Fat-like and Dachsous are planar polarized, providing a demonstration of planar polarization of proteins in a nonbilaterian organism. We also discover roles for *Hydra* Fat-like in cell adhesion, spindle orientation, and tissue organization.

Author contributions: M. Brooun and H.M. designed research; M. Brooun and A.K. performed research; A.K., M. Bashkurov, and B.J.P. contributed new reagents/analytic tools; M. Brooun and H.M. analyzed data; and M. Brooun, R.E.S., and H.M. wrote the paper.

The authors declare no competing interest.

This article is a PNAS Direct Submission.

[1]To whom correspondence may be addressed. Email: brooun@lunenfeld.ca or mcneillh@wustl.edu.

This article contains supporting information online at https://www.pnas.org/lookup/suppl/doi:10.1073/pnas.1917570117/-/DCSupplemental.

First published July 29, 2020.

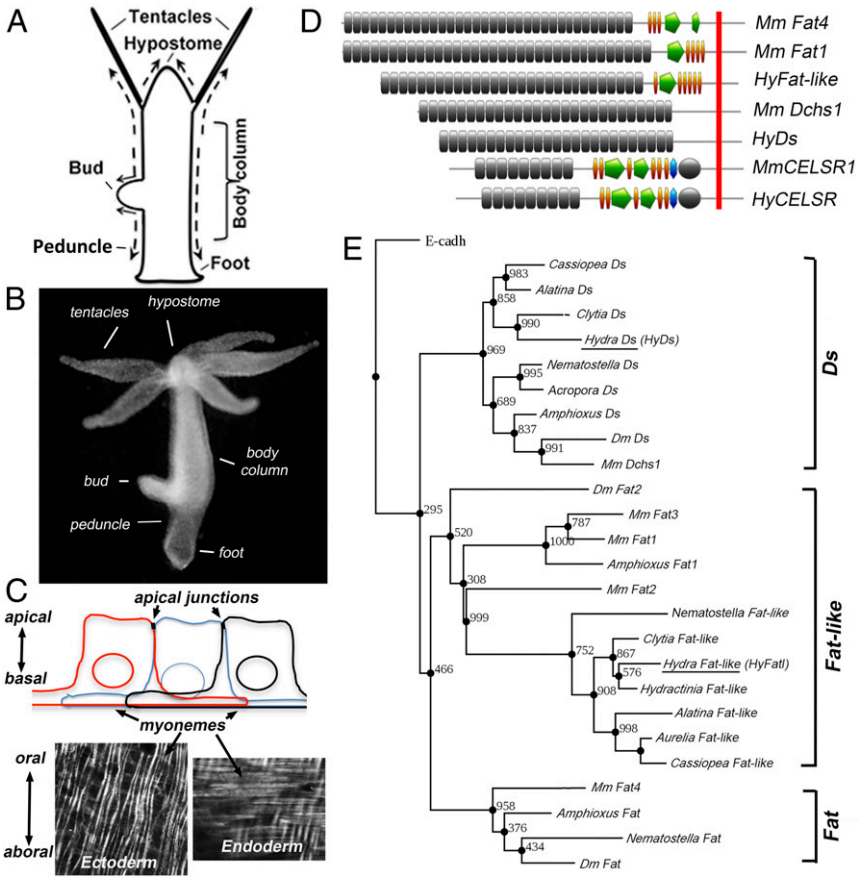

Fig. 1. Cnidarian *Hydra* possesses single homologs of atypical cadherins Fat-like, Ds, and CELSR. (*A*) Schematic of the *Hydra* body plan, arrows indicate directions of cell displacement. (*B*) Budding adult *Hydra* polyp. (*C*) Schematic (lateral view) of ectodermal epithelial cells of *Hydra* with confocal images of ectodermal and endodermal myonemes stained with phalloidin. (*D*) Domain composition of representative atypical cadherins. , cadherin domain; , EGF repeat-like domain; , laminin domain; , hormone receptor domain; , latrophilin/CL-1-like GPS domain; and , cellular membrane. (*E*) Phylogenetic tree of Fat, Fat-like, and Ds subfamilies based on the ICD sequence, maximum likelihood analysis (1000 bootstrap replicates, bootstrap values are indicated for each node) supports the clustering of the predicted *Hydra* homologs (underlined) with the Fat-like and Ds cadherin subfamilies. Alignments were done using MAFFT (https://www.ebi.ac.uk/Tools/msa/mafft/). Mm, *Mus musculus*; Dm, *Drosophila melanogaster*.

module is acting in those locations. However, in the body column of *Hydra*, despite planar polarization of myonemes, oriented cell division and directional displacement of epithelial cells (Fig. 1 *A* and *C*) (18), expression of core PCP genes is low (15), suggesting that another planar polarity mechanism could be acting there.

Here we characterize Fat-like (HyFatl) and Ds (HyDs) cadherins in *Hydra*. We show that a Fat-like cadherin regulates tissue organization in a nonbilaterian animal. Both HyFatl and HyDs are apically localized in epithelial cells and are planar polarized along the oral–aboral axis. These data indicate that planar polarization of Fat-like and Dachsous cadherins evolved prior to the divergence of cnidarians and bilaterians. No Fat/Fat4 homolog exists in *Hydra*. We show polarization of HyFatl is dynamic and increases in areas where cell displacement rates are high. Reduction of HyFatl leads to disruption of cell contacts and morphology of actin cables in myonemes. Overexpression experiments indicate the intracellular domain of HyFatl is involved in actin organization and oriented cell division. Transgenic knockdown experiments indicate that *HyFatl* plays a role in tissue level organization in the body column.

Results

***Hydra* Possesses Single Homologs of Fat-like, Ds, and CELSR Cadherins.** Cadherins of the Fat-like (*Mm* Fat1 and Fat3, *Dm* Fat2) and true Fat (*Mm* Fat4, *Dm* Fat) families have a characteristic domain composition (Fig. 1*D*). Our analysis of *Hydra* genomic, transcriptomic, and expressed sequence tag (EST) data identified only a single *Fat-like* cadherin gene (*HyFatl*) and a single *Ds* gene (*HyDs*), with no true Fat homolog. HyFatl and HyDs have a similar structure as their vertebrate orthologs Fat1 and Dchs1 (Fig. 1*D*). However, the intracellular domains (ICDs) of HyFatl and HyDs show only low similarity with *Drosophila* and vertebrate homologs (14% for HyFatl, 18% for HyDs) (*SI Appendix*, Fig. S1 *A* and *E*), and higher similarity with orthologs from the medusozoan group of cnidarians (26 to 55% for HyFatl, 21.1 to 29.3% for HyDs) (*SI Appendix*, Fig. S1 *D* and *E*).

The ICDs of cnidarian Fat-like proteins have three proline-rich motifs (*SI Appendix*, Fig. S1 *A* and *D*), which have homology to EVH1-binding domains of *Mm*Fat1 (8, 20), suggesting a role for HyFatl in the regulation of actin organization. HyFatl ICD also shares a short three amino acid sequence motif—HWD—with *Mm*Fat1 and *Mm*Fat3 (*SI Appendix*, Fig. S1*A*). This sequence is part of a larger domain that contributes to the kinesin-mediated apical localization of Fat3 in Madin-Darby Canine Kidney (MDCK) cells (21). HWD is present in the ICDs of most Fat-like proteins, but not in ICDs of Fat, Ds, CELSR, or classical cadherin protein families.

Phylogenetic analysis of HyFatl using either the intracellular domain (Fig. 1*E*) or the extracellular domain (*SI Appendix*, Fig. S1*F*) reveal homology with *Drosophila* Fat2 (also known as Fatlike and Kugelei) and the mammalian Fat-like cadherins Fat1, Fat2, and Fat3. In contrast, alignment of HyFatl with true Fats (*Mm*Fat4 and *Dm*Fat) reveals a lack of conserved domains and low similarity (10.8%) (*SI Appendix*, Fig. S1*B*). Alignment of

HyFatl with Fat from *Nematostella vectensis* (10), also shows low similarity (11.8%) (*SI Appendix*, Fig. S1*C*). Thus, while *Nematostella* has a Fat and a Fat-like cadherin, *Hydra* has only a single Fat-like protein, and no Fat/Fat4 homolog.

Hydra Ds has regions of similarity in the ICD with bilaterian Ds orthologs, most strikingly in a region partially overlapping HR2 (*SI Appendix*, Fig. S1*E*, double underlined) (22, 23). However, although conservation of the Ds ICD is clearest among three homology regions (HR1 to HR3) in bilaterian Ds (10), these regions are not present in ICD of HyDs nor in Ds homologs of the medusozoans *Clytia*, *Alatina*, or *Cassiopea* (*SI Appendix*, Fig. S1*E*).

Thus, analysis of domain compositions as well as phylogenetic analyses using either sequences comprising all cadherin domains or ICDs confirm that these cadherins belong to Fat-like and Ds families (Fig. 1 *D* and *E* and *SI Appendix*, Fig. S1*F*). A true Fat homolog is present in the anthozoan cnidarians *Nematostella* and *Acropora* (24). However, we were unable to identify a homolog of Fat in *Hydra* or other medusozoan cnidarians. Analysis of proteins that were automatically annotated as *Hydra* Fat homologs in the National Center for Biotechnology Information (NCBI) GenBank revealed that their domain compositions differ from Fat family proteins (*SI Appendix*, Fig. S1*G*) and their intracellular domains are much shorter (69 to 157 amino acids) than Fat cadherins (456 to 542 amino acids), with no sequence similarity (10). Our in silico analysis also revealed a single *Hydra* homolog of Flamingo/CELSR, another atypical cadherin involved in PCP (25), that we call HyCelsr (*SI Appendix*, Fig. S1*H*). We conclude that *Hydra* has single orthologs of Fat-like, Ds, and CELSR cadherins, but does not have a Fat/Fat4 homolog.

HyFatl and HyDs Are Planar Polarized in the Body Column. In situ hybridization shows that in adult *Hydra* polyps *HyFatl* and *HyDs* are expressed in ecto- and endodermal epithelial cells throughout the body column, with weaker expression in the tentacles and hypostome (*SI Appendix*, Fig. S2). *HyFatl* expression is strongest in the lower portion of the body column, just above the foot, and in the tentacle bases.

To examine HyFatl cellular localization, we generated polyclonal antibodies against HyFatl ICD (residues 4,191 to 4,393). Immunoblotting of *Hydra* lysates with anti-HyFatl antiserum identified a polypeptide of ∼490 kDa, corresponding to the predicted molecular weight of full-length HyFatl. In addition, polypeptides of ∼180 kDa and 100 kDa were specifically recognized by this antiserum (Fig. 2*E*). Because Fat and Fat-like cadherins have been shown to be posttranslationally cleaved (26–29), HyFatl may also undergo proteolytic processing which could explain the lower molecular weight fragments. When HyFatl antisera was preabsorbed with HyFatl-GST, but not GST (Fig. 2*E*), these bands were no longer recognized, supporting specificity.

Immunostaining of fixed *Hydra* polyps with HyFatl antiserum and affinity-purified anti-HyFatl antibodies revealed strong expression of HyFatl at apical ectodermal epithelial junctions (Fig. 2 *A–D*). HyFatl is also present at the basal membrane along the myonemes of ectodermal epithelial cells and along the lateral membranes of endodermal epithelial cells (*SI Appendix*, Fig. S3 *A*, *D*, and *G*). In this study we focus on the expression of HyFatl in the ectoderm, where expression is strongest.

HyFatl staining accumulates strongly at tricellular apical junctions throughout the body column (Fig. 2 *A*, *D* and *F*), similar to *Drosophila* Fat2/Fat-like (7, 30, 31). Significantly, HyFatl staining is higher in membranes that are perpendicular to the oral–aboral axis of the animal (Fig. 2 *B*, *C*, and *H* and *SI Appendix*, Fig. S3 *J* and *K*), suggesting HyFatl is planar polarized along the oral–aboral axis. To measure the degree of polarization, we calculated a polarization value (PV) of HyFatl, the ratio between intensity of staining of the apical membrane most perpendicular to the oral–aboral axis and the membrane most aligned with the oral–aboral axis (Fig. 2*H*). Interestingly, planar polarized localization of HyFatl was seen in elongated cells of the body column, but not in the head or peduncle regions where the apical surfaces of ectodermal epithelial cell are rounded (Fig. 2 *A–D* and *H* and *SI Appendix*, Fig. S3*L*). Both ecto- and endodermal HyFatl staining were lost when the antiserum was preabsorbed with HyFatl-GST, but not GST (Fig. 2 *F* and *G* and *SI Appendix*, Fig. S3 *A–I*), supporting antibody specificity. Interestingly, neither claudin, nor FGF2 (32) (membrane markers for *Hydra* ectodermal epithelial cells) are planar polarized in the body column (*SI Appendix*, Fig. S3 *M–O*), suggesting that oral–aboral planar polarization is not a general feature of *Hydra* membrane proteins.

We also generated antibodies against HyDs ICD (residues 2,958 to 3,113). Immunostaining with an affinity-purified HyDs antibody revealed a similar pattern as anti-HyFatl at apical junctions of ectodermal epithelial cells (Fig. 2 *I–K*). HyDs is also enriched at the tricellular junctions and at the apical membranes perpendicular to the oral–aboral axis. Similar to HyFatl, polarized accumulation of HyDs along the apical membrane was observed only in the body column, not in the peduncle or hypostome (Fig. 2*N* and *SI Appendix*, Fig. S3*L*). The specificity of junctional staining of HyDs antibody was confirmed by preabsorbing with HyDs-GST antigen (Fig. 2 *L* and *M*). Thus both HyFatl and HyDs are planar polarized in the oral–aboral axis in the body column.

Planar Polarization of HyFatl Is Highest in Ectodermal Epithelial Cells that Undergo Directional Displacement. Planar polarization of Fat-like proteins has been linked to their role in directional cell migration and asymmetric cell morphology in bilaterians (6, 8, 30, 31, 33). Interestingly, polarization of HyFatl is observed only in the body column where cells undergo continuous oriented cell division and displacement toward the head and the foot (Figs. 1*A* and 2*H*). In the hypostome and peduncle, where the rate of epithelial cell displacement is much lower (17), the polarization of HyFatl is lower as well. We hypothesized that HyFatl becomes polarized when ectodermal epithelial cells are coordinately displaced.

The generation of a new bud in *Hydra* provides a system for examining the effects of changes in the rates of cell displacement on HyFatl (34). Cells that are being recruited into new bud tissue undergo extensive rearrangements, and their rate of displacement and junctional remodeling is significantly higher than in the maternal body column (35). During bud development, cells of the body column move coordinately into the growing bud, change their orientation, and align along a new oral–aboral axis, that is perpendicular to the maternal axis (35) (Fig. 3*A*). At budding stages 2 and 3, cells of the body column that are recruited into a new bud lose planar polarization of HyFatl (Fig. 3*B*). As the bud develops, at stages 4 to 7, HyFatl remains unpolarized at the tip of the bud, the future head cells. However, in the growing body column of the bud and in cells being displaced from the parent into the bud, HyFatl is polarized along the bud's oral–aboral axis (Fig. 3 *B* and *C*). HyFatl polarization in those cells was also higher than in the cells of a maternal body column (Fig. 3 *C* and *D*). Thus HyFatl polarization correlates with rate of cell displacement during budding.

In order to examine HyFatl polarization in situations when the rate of displacement of epithelial cells is low we next examined the effects of starvation. Starvation slows down the cell cycle and the rate of epithelial cell displacement in the body column (36, 37). Significantly, starvation for 5 d resulted in a decrease in HyFatl polarization (Fig. 3 *C* and *E*).

We also examined HyFatl staining during aggregation. *Hydra* can be dissociated into a suspension of single cells, which, when aggregated, give rise to new animals (Fig. 3*F*) (38). Forty-eight

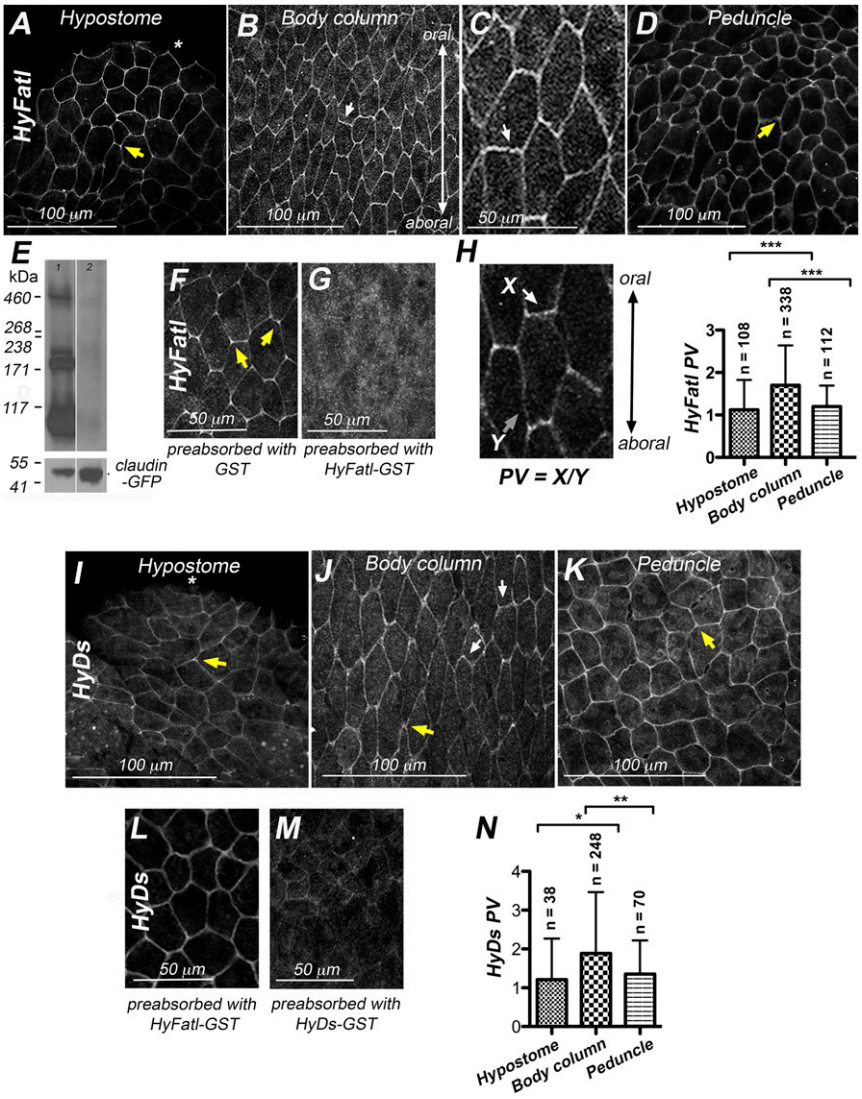

Fig. 2. HyFatl and HyDs are expressed at apical junctions of ectodermal epithelial cells in a planar polarized manner. White arrows indicate immunostaining of apical membranes perpendicular to the oral–aboral axis, yellow arrows indicate immunostaining at tricellular junctions, and asterisk indicates tip of the hypostome. (*A*–*D*) Apical views of ectoderm immunostained with anti-HyFatl serum. (*E*) Immunoblot analysis of total protein lysate from a transgenic *Hydra* line constitutively expressing claudin-GFP; HyFatl anti-serum was preabsorbed with either GST (lane 1) or GFT-HyFatl antigen (lane 2); presented lanes are a selection from the original image. (*F* and *G*) Apical view of ectoderm immunostained with a HyFatl anti-serum that was preabsorbed with (*F*) GST protein or (*G*) HyFat-GST antigen. (*H*) Calculation of a polarization value (PV) for immunostained epithelial cell; gray arrow points to the apical membrane parallel to the oral–aboral axis; graph shows PVs of HyFatl in different parts of the *Hydra* body. (*I*–*K*) Apical view of the ectoderm immunostained with affinity-purified anti-HyDs antibodies. (*L* and *M*) Apical view of ectoderm immunostained with affinity-purified anti-HyDs antibodies preabsorbed with (*L*) HyFatl-GST or (*M*) HyDs-GST antigens. (*N*) PVs of HyDs in different parts of the *Hydra* body. In *H* and *N* data shown as mean with SD, two-tailed *t* test; for each measurement three to five animals were used; ***$P < 0.0001$, **$P = 0.0074$, *$P = 0.0113$; the spread of the data points is shown in *SI Appendix*, Fig. S3*L*.

hours after dissociation, aggregates form a hollow sphere with ecto- and endodermal layers; however, new axes are not yet present and there is no organized displacement of epithelial cells. In these conditions HyFatl is visible at the apical junctions, but is not polarized (Fig. 3*F*). As the polyps forming from the aggregates elongate, HyFatl becomes polarized again along the oral–aboral axis. Taken together, these data suggest that HyFatl becomes planar polarized in the direction of epithelial cell displacement and this polarization increases with the rate of displacement.

Ectopic Expression of HyFatl ICD Disrupts Organization of the Actin Cytoskeleton via EBM Motifs. MmFat1 and MmFat3 cadherins promote cell migration and polarization through regulation of actin polymerization and microtubule alignment via their intracellular domains (6, 8, 21, 33). Examination of the intracellular domain of HyFatl revealed the presence of three EVH1 binding motifs (EBMs), similar to those found in mammalian Fat1 and Fat3, which have been suggested to regulate actin dynamics (6, 8, 33) (*SI Appendix*, Fig. S1 *A* and *D*). To explore the role of the intracellular domain of HyFatl and the EBM motifs, we generated two transgenic *Hydra* lines: *ICD* constitutively expressed GFP-tagged HyFatl ICD (residues 4,100 to 4,392) and *dICD* constitutively expressed an ICD constructs lacking all three EBMs (Fig. 4*A*). Transgenic *Hydra* were obtained by injecting plasmid DNA into one- to four-cell-stage embryos (39). Fully transgenic *ICD-GFP* and mosaic *dICD-GFP* lines (denoted *ICD* and *dICD*, respectively) were established. Mosaic *dICD* animals with the transgene expressed in at least 20% of ectodermal epithelial cells were used for experiments. Transgenic cells of interstitial lineage were not detected in either line.

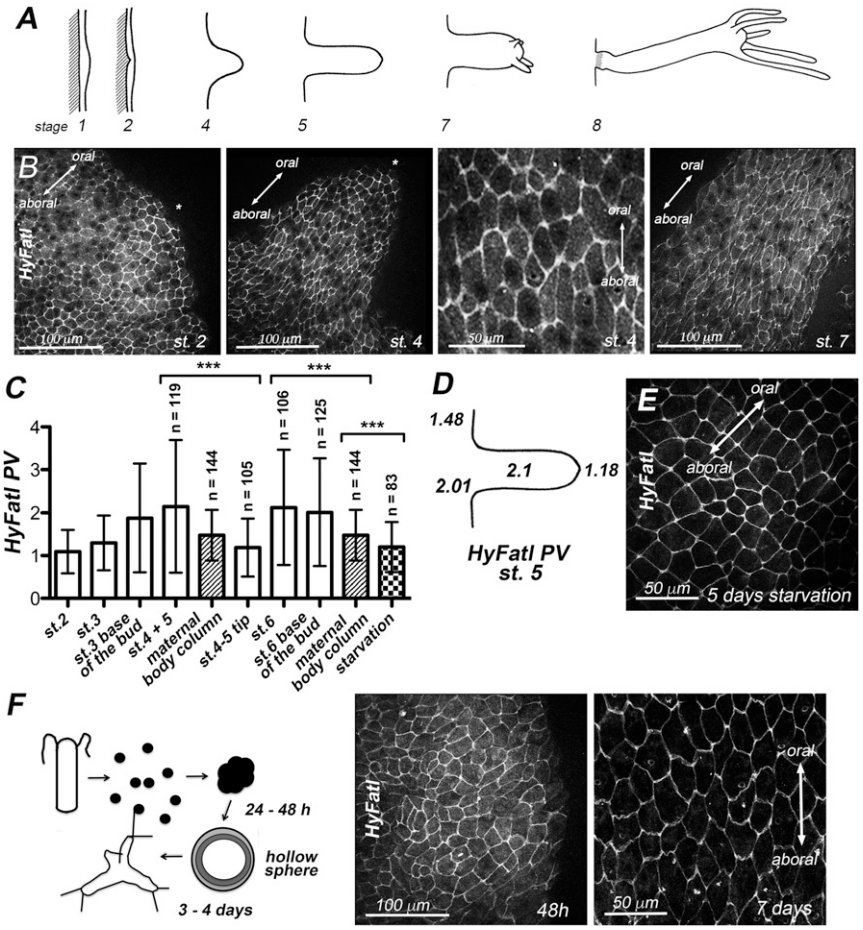

Fig. 3. Planar polarization of HyFatl increases in ectodermal epithelial cells that undergo displacement. (*A*) Schematic of bud development is adapted from ref. 34. (*B*) Dynamic of HyFatl localization during bud development; asterisk indicates the tip of the bud. At stage 2 (st. 2), HyFatl polarization is lost and it increases at the following stages. (*C*) PV of HyFatl of the body column during budding and after 5 d of starvation; the "maternal body column" bar is duplicated for better visualization. Stages 4 and 5 were combined; during these stages, cells of the maternal body column continue to move into the growing bud (34), therefore, from the point of tissue dynamics these stages are similar and can be combined. Mean with SD, one-way ANOVA (***$P < 0.0001$) and two-tailed *t* tests (***$P = 0.0009$), three to four animals for each group; data for individual animals used in the analysis are presented in *SI Appendix*, Fig. S3*P*. (*D*) Schematic of polarization values of HyFatl determined for st. 5 bud, PV of the body column cells (1.48) increases as they are being recruited into the bud tissue (2.01), stays high in the body column of a bud (2.1), and drops at the tip of the bud (1.18). (*E*) Apical view of ectoderm of *Hydra* starved for 5 d immunostained with anti-HyFatl; HyFatl is not polarized. (*F*) Schematic of *Hydra* aggregate development and apical view of 48-h and 7-d-old aggregate immunostained with anti-HyFatl; in 48-h-old aggregate no polarization of HyFatl is visible; statistical analysis is provided in *SI Appendix*, Fig. S3*Q*.

The body shape of fully transgenic *ICD-GFP* polyps (denoted *ICD*) and polyps mosaic for *dICD* animals (20 to 60% mosaic) was normal. Costaining with antibodies to GFP and HyFatl showed that ICD-GFP and dICD-GFP are enriched along apical junctions, while in controls GFP is not (Fig. 4 *B*–*D*′). This suggests that sequences in the ICD aside from the EBMs mediate recruitment to apical junctions. The shape of both *ICD*- and *dICD*-expressing cells in the body column were more circular compared to more elongated control cells (Fig. 4 *B*–*E*). Interestingly, there was also a clear correlation between the circularity of the cell and polarization of HyFatl in the control animals, with more elongated cells having more polarized HyFatl (*SI Appendix*, Fig. S4*A*).

Since the HyFatl antibody recognizes both endogenous and ectopic HyFatl, we could not determine if overexpression of HyFat-ICD altered polarization of endogenous HyFatl. We could, however, test if planar polarization of HyDs is affected in *ICD* cells. HyDs shows planar polarization in the absence or presence of ectopic HyFatl, indicating that ICD of HyFatl does not alter HyDs polarization. There were occasional increases of HyDs staining in ICD expressing cells, but those differences were not significant (*SI Appendix*, Fig. S4*B*).

To examine the junctional actin cytoskeleton, control and transgenic animals were stained with phalloidin. The intensity of phalloidin staining at the apical junctions was not significantly different between control polyps and *ICD* and *dICD* transgenics (*SI Appendix*, Fig. S4 *C* and *D*). Thus, overexpressed HyFatl ICD does not alter junctional actin distribution.

The apical surface of ectodermal cells has thin phalloidin-positive microvilli. Strikingly, multiple, elongated microvilli were observed on the apical surface of the *ICD* ectoderm (Fig. 4*F*), and both their length and number were significantly higher than in control (Fig. 4 *F*, *H*, and *I*). In contrast, *dICD* cells had significantly fewer and shorter apical microvilli (Fig. 4 *H* and *I*) than animals expressing ICD-GFP. These data suggest that overexpression of HyFatl can alter actin rich microvilli in an EBM-dependent manner.

We also noticed that nuclei of ectodermal epithelial cells, that are normally located in the basal half of the cell, had an abnormal apical position in *ICD* cells (Fig. 4 *G* and *J*), but not in *GFP* or *dICD* cells.

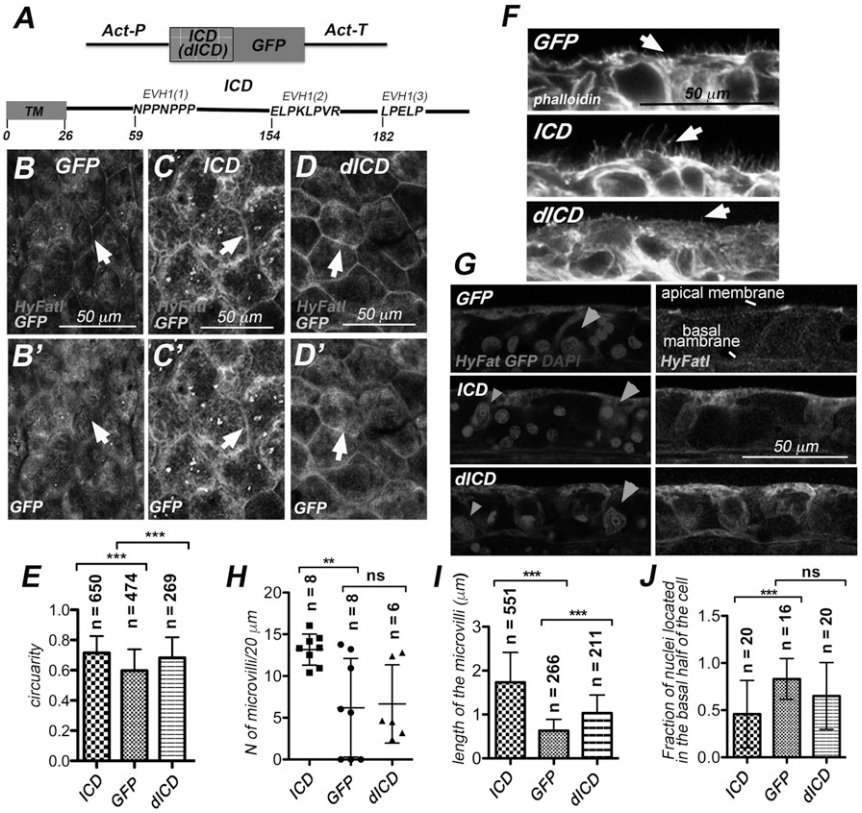

Fig. 4. Ectopic expression of HyFatl ICD interferes with actin organization. (*A*) Schematic of the ICD(dICD)-GFP construct; in the schematic of TM-ICD (TM, transmembrane domain), three proline-rich potential EBMs deleted in dICD are indicated. (*B–D′*) Apical view of ectodermal epithelial cells immunostained with anti-HyFatl and anti-GFP antibodies; arrows indicate apical junctions. (*E*) Circularity of the control and transgenic ectodermal epithelial cells, Mean with SD, two-tailed *t* test, ***$P < 0.0001$, four to six animals of each line. (*F*) Microvilli (arrows) on the apical surface of the ectodermal epithelial cells visualized with phalloidin; lateral view of the ectoderm. (*G*) Lateral view of ectoderm immunostained with anti-GFP and anti-HyFat demonstrates recruitment of ICD-GFP and dICD-GFP to the apical surface; arrowheads indicate epithelial nuclei; note epithelial nucleus of ICD cell in the apical position. (*H*) Number of microvilli on the apical surface calculated per 20 μm of a confocal image. Mean with SEM for n confocal images, one-way ANOVA, four to five animals of each line; numbers of microvilli are significantly different in *ICD* and *dICD* (**$P < 0.0036$); ns, no significant difference. (*I*) Length of microvilli. Mean with SD, two-tailed *t* test, four to five animals of each line; lengths of microvilli in *ICD* and *dICD* are significantly different ($P < 0.0001$). (*J*) Fraction of ectodermal epithelial nuclei located in the basal half of a cell. N, number of confocal images, five animals of each line, mean with SD, two-tailed *t* test, ***$P < 0.001$.

Ectopic Expression of HyFatl ICD Affects Oriented Cell Division. Because oriented cell division can be regulated by PCP, we examined orientation of the mitotic spindle in *Hydra* that overexpress HyFatl-ICD. Anti-Phospho-Histone H3 staining was used to visualize cells in metaphase and anaphase and to determine orientation of the mitotic spindle (Fig. 5 *A* and *B*). *Hydra* ectodermal epithelial cells divide in the direction of the oral–aboral axis (18). The mean angle between the mitotic spindle of ectodermal cells in *GFP* controls (32°) was not significantly different from the wild-type *AEP* strain (29°) (Fig. 5*F*) and similar to published data (33°) (18). Importantly, however, in *Hydra* that overexpress HyFatl ICD, the spindle angle of *ICD* cells was less tightly linked with the oral–aboral axis (49°) (Fig. 5 *C*, *D*, and *F*). The mean spindle angle of *dICD* cells (38°), however, did not differ significantly from controls (Fig. 5 *E* and *F*). Thus, ectopic expression of HyFatl ICD affects orientation of the mitotic spindle, and this effect is diminished if the EBMs are deleted.

Down-Regulation of *HyFatl* Affects Adhesion. Next, we sought to inactivate *HyFatl* using an RNA hairpin approach (40). Two different hairpin-expressing sequences, *shFatl9* (nucleotides 12,573 to 13,178) and *shFatl4* (nucleotides 11,493 to 11,792) were inserted downstream of GFP under control of an actin gene promoter that is active in all epithelial cells (41) (Fig. 6 *A*, *Top*). We could not obtain stable transgenic lines expressing the hairpins under control of the actin promoter because hatchlings rapidly lost transgenic cells. These data suggest that the down-regulation of *HyFatl* caused by constitutive expression of the hairpins led to loss of cells. Only one line bearing the *GFP-shFatl4* survived for a month. To overcome the lethality of *shFatl* knockdown, we cloned *shFatl9* hairpin into the doxycycline-inducible vector pIndGFP (Fig. 6 *A*, *Bottom*). We were able to establish one *Hydra* line that expressed low levels of the *shFatl9* hairpin, constitutively, without induction by doxycycline (*SI Appendix*, Fig. S5). We made multiple attempts to establish additional lines; however, expression of the marker of the transgenic vector was consistently lost. These data suggest that strong inhibition of HyFatl leads to cell loss and is lethal to the animal.

shFatl9 polyps show loss of *HyFatl* transcript by in situ hybridization (Fig. 6 *B* and *C*). Immunoblotting showed consistent decreases in HyFatl protein in *shFatl9* polyps (Fig. 6*D*). Immunostaining of *shFatl9* and *shFatl4* animals with HyFatl antiserum also showed reduced levels of HyFatl along the membranes of ectodermal epithelial cells and at tricellular junctions (Fig. 6 *G–I*), further validating the HyFatl antibody. However, residual staining indicated that knockdown of *HyFatl* in *shFatl9* and *shFatl4* polyps was incomplete.

Analysis of *shFatl9* partial knockdown animals revealed several phenotypic features. Transgenic animals bearing an empty vector were used as controls. The body column of *shFatl9* was notably elongated compared with controls and had a "lumpy

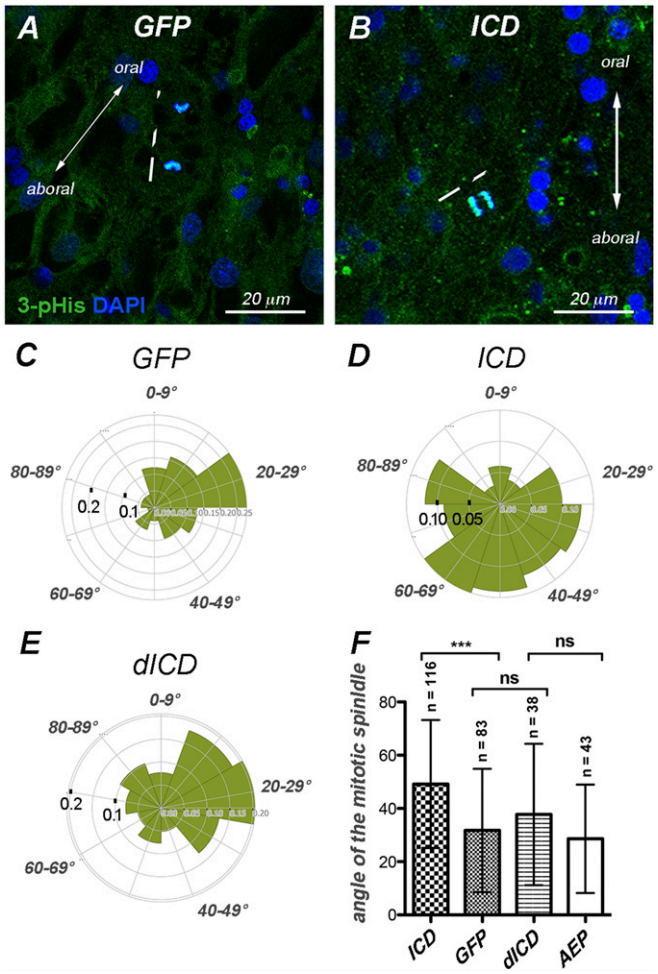

Fig. 5. Ectopic expression of HyFatl ICD interferes with mitotic spindle orientation. (*A* and *B*) Confocal images of ectodermal epithelial cells in anaphase immunostained with anti-phospho-Histone H3 antibodies. Dashed lines indicate the orientation of mitotic spindles. (*C*–*E*) Distribution of angles between the mitotic spindles and oral–aboral axis shown as a fraction. (*F*) Graph showing the angles between the mitotic spindles and oral–aboral axis. Mean with SD, two-tailed *t* test, (***$P < 0.0001$), number of animals used for analysis: GFP, 12; ICD, 17; dICD, 8; and AEP, 2.

sock" appearance (Fig. 6 *E* and *F*). We did not observe an altered body shape with *shFatl4*, likely due to the smaller number of transgenic cells. The apical contacts between ectodermal epithelial cells of *shFatl9* and *shFatl4* often become separated upon fixation (Fig. 6 *H* and *I*). The number of such broken cell–cell contacts was significantly higher in *shFatl9* animals in comparison with both controls and *ICD* animals (Fig. 6*J*). This suggests that loss of HyFatl weakens cell–cell adhesion. Although the *shFatl9* line was more stable than *shFatl4,* elimination of transgenic cells occurred in *shFatl9* polyps as well: we often observed multicellular junctions resembling healing wounds along the body column of *shFatl9* animals (*SI Appendix*, Fig. S6). We propose that they are the result of healing at sites where cells have been lost. Over time, the *shFatl9* line had reduced viability and was also lost. Taken together, these data suggest that *HyFatl* is required for cell–cell adhesion.

Down-Regulation of *HyFatl* Affects Cell Alignment and Apical Surface Area of Ectodermal Epithelial Cells. Epithelial cells in the *Hydra* body column are a sheet of similar-sized cells with the axes of their longest dimensions oriented in the same direction. However, in *shFatl9*, *shFatl4*, *ICD*, and *dICD* animals, epithelial ectodermal cells were misaligned (Fig. 7 *A*–*D*). This misalignment was also observed in the endoderm of *shFatl9* (Fig. 7 *E* and *F*), where *HyFatl* was partially inactivated (see in situ hybridization and immunoblot analyses) (Fig. 6 *B*–*D*).

In *shFatl* knockdowns, epithelial cells also differed from each other in size. This difference was especially obvious in the basal disk (Fig. 7 *G* and *H*) where HyFatl is highly expressed but unpolarized. We used a "neighbor" method (*Materials and Methods*) to measure the degree of cell misalignment and cell size difference. In the body column in control polyps, neighboring cells have a similar size and orientation. The orientation of *shFatl* knockdowns, *ICD*, and *dICD* cells is irregular, although the phenotype is less penetrant in *ICD* and dICD cells (Fig. 7*I*). Cell size is significantly different in *shFatl* knockdowns, but not in *ICD* or *dICD* cells (Fig. 7*J*). Interestingly, *shFatl9* cells are more rounded than controls, resembling the phenotype of *ICD* and *dICD* cells (Figs. 4*E* and 7*K*). Since shape is altered in both *shFatl* knockdowns and *ICD* and *dICD* cells, the observed misalignment could be due to altered shape. Shape, orientation, and circularity of cells expressing a control hairpin for *FoxO* (40) are not altered (Fig. 7 *I*–*K*).

Down-Regulation of HyFatl Alters the Actin Cytoskeleton. *Hydra* myonemes are contractile processes located on the basal side of epithelial cells, attached to the mesoglea (Fig. 1*C*) (42). A manifestation of PCP in *Hydra* is the parallel arrangement of ectodermal myonemes along the oral–aboral axis. HyFatl is weakly detected along the ectodermal myonemes (*SI Appendix*, Fig. S3 *A*, *B*, *D*, and *E*). We examined whether down-regulation of *HyFatl* or ectopic expression of HyFatl ICD affects the alignment of ectodermal myonemes. Myonemes in *shFatl9 Hydra* were still oriented in the oral–aboral direction. However, actin cables in the myonemes were less straight than in controls and had a "frizzled" appearance (Fig. 8 *A* and *B*). Actin cables in *ICD* cells looked somewhat thicker but otherwise normal (Fig. 8*C*). We also examined if abundance of polymerized actin is changed in *shFatl9* cells. Staining of control and *shFatl9* animals with phalloidin did not reveal any significant changes (*SI Appendix*, Fig. S6*B*). Thus, down-regulation of *HyFatl* affects the morphology of actin bundles, but does not have an effect on the actin at apical junctions.

Discussion

Our results indicate that the function of Fat-like cadherins in organizing cells and tissues was established early in animal evolution. Both gain-of-function and loss-of-function studies implicate *Hydra* Fat-like in cell–cell adhesion and actin organization. Remarkably, we also find that both HyFatl and HyDs are planar polarized in the body column of *Hydra*. This is a demonstration of planar polarization of a protein in a nonbilaterian. Fat and Ds proteins in bilaterians have been intensively investigated, and their asymmetric localization is thought to be crucial for their role in planar polarization of tissues (reviewed in ref. 43). Planar polarization of Fat-like proteins has also been observed and is linked to their role in directional cell migration and asymmetric cell morphology (8, 30, 31, 33, 44).

HyFatl is planar polarized at epithelial membranes that are perpendicular to the oral–aboral axis. It is also enriched at tricellular junctions, similar to *Drosophila* Fat2 (7, 30, 31). However, we note that the planar polarization of HyFatl is not as strong as *Drosophila* Fat2. We find that HyFatl is localized along the total length of apical junctions, although clearly enriched at oral–aboral membranes. This might reflect its additional function in cell adhesion: partial knockdown of HyFatl leads to weakening of the cell–cell contacts. Cells are also rapidly lost from transgenic lines with strong knockdown of *HyFatl*, also consistent with a role of HyFatl in cell adhesion. Importantly, where cells are

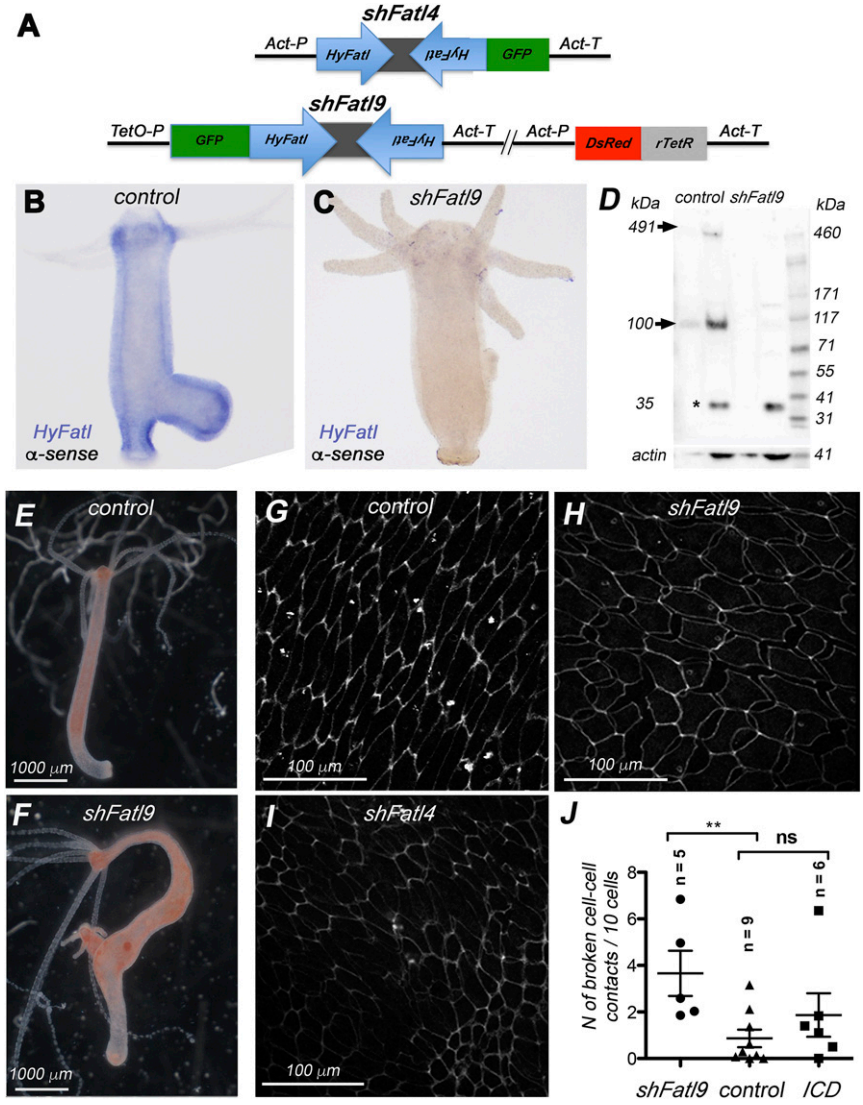

Fig. 6. Down-regulation of *HyFatl* affects the adhesion of ectodermal epithelial cells. (*A*) Schematic of constitutive (*Top*) and doxycycline-inducible (*Bottom*) *shFatl* constructs in pIndGFP vector. (*B* and *C*) In situ hybridization with *HyFatl* antisense and sense probes. (*D*) Immunoblot analysis with affinity-purified anti-HyFatl antibodies of lysate from control and *shFatl9* polyps. Arrows indicate the full length and 100 kDa HyFatl; asterisk indicates a nonspecific 35 kDa band. (*E* and *F*) *shFatl9* mutant has an altered body column shape. (*G–I*) Immunostaining of the ectoderm with anti-HyFatl antibodies reveals weaker adhesive contacts and irregularly shaped epithelial cells in *shFatl9* and *shFatl4* polyps. (*J*) Graph showing the number of broken cell–cell contacts per 10 cells. n, number of animals used for analysis; mean with SEM (**$P = 0.0073$). The total number of cell pairs scored was 1,294 for the control, 356 for *shFatl9*, and 996 for *ICD*.

not polarized, such as the foot, HyFatl still functions, as seen as increased size variability in knockdown conditions.

Planar polarization of HyFatl is most notable in epithelial cells undergoing displacement, but not in the foot or hypostome, where the speed of an epithelial cell's displacement is lower than in the body column (17). HyFatl polarization increases further in the growing bud and is reduced in starved animals and in early stage aggregates, where cell displacement is slowed down or stopped. This dynamic nature of HyFatl localization is also reminiscent of *Drosophila* Fat2 during egg chamber rotation: normally planar polarized along the migrating epithelium, Fat2 loses its polarization in eggs with migration defects (30).

Oriented cell division can be regulated by planar polarity signaling in bilaterians (1). Our studies raise the possibility that planar polarization of HyFatl may have a role in oriented cell division in *Hydra* because we find that ectopic expression of the intracellular domain of HyFatl results in less precise orientation of the mitotic spindle. Because our studies indicate that loss and gain of function of HyFatl affects cell adhesion and the cytoskeleton, we cannot be sure if this PCP phenotype is due to a role for HyFatl in PCP, or indirectly due to alterations in cell adhesion and the actin cytoskeleton. Both reduction of *HyFatl* and overexpression of HyFatl ICD led to rounding of cells, suggesting that overexpression of ICD might have some dominant negative effects.

Mammalian Fat1 and Fat3 promote cell migration and polarization through regulation of actin and microtubule alignment via interactions of their intracellular domains with Ena/VASP (6, 8, 33) binding EBM motifs. Interestingly, despite low overall identity with bilaterian homologs, knockdown or overexpression of HyFatl alters the actin cytoskeleton, and this effect is reduced by deletion of EBMs. Down-regulation of *HyFatl* affected the morphology of actin bundles in the ectodermal myonemes (Fig. 8*B*), leading to a frizzled appearance. Overexpression of HyFatl ICD led to increased actin rich microvilli at the apical surface, mediated at least in part by the EBMs. HyFatl is not normally

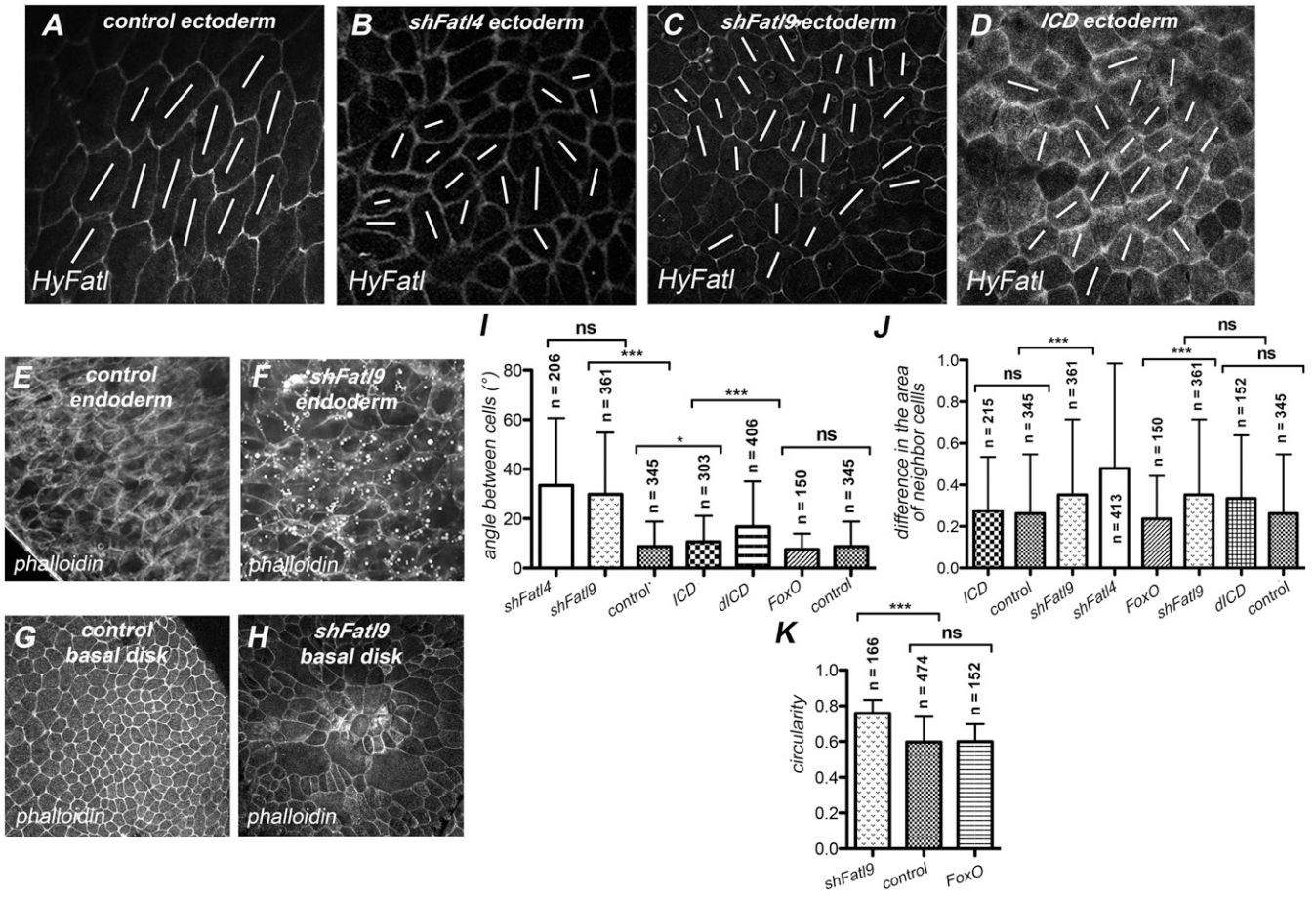

Fig. 7. Alignment of ectodermal epithelial cell and surface area altered in *shFatl* transgenics. (*A–D*) Apical view of ectodermal cells immunostained with anti-HyFatl. (*E* and *F*) Confocal images of an endoderm stained with phalloidin, misalignment of *shFatl9* endodermal cells is visible. (*G* and *H*) Apical view of the ectodermal surface of the basal disk stained with phalloidin demonstrates the differences in *shFatl9* cell surface area. (*I*) Graph showing the mean angle between the longest dimensions of neighbor cells, mean with SD, two-tailed *t* test; differences between control and *shFatl9* and control and *ICD* are significant (***$P < 0.0001$, *$P = 0.0161$). (*J*) Graph showing differences in the surface area of neighbor cells using the neighbor method. Orientation of individual cell was calculated as the angle between the longest axis of the cell surface and the arbitrary direction using MATLAB. To evaluate differences in the surface area for each pair of neighboring cells, the ratio of the surface area S_n/S_{n-1} was calculated, subtracted from 1, and the absolute value abs$[1 - S_n/S_{n-1}]$ was used to measure the degree of heterogeneity in the apical surface area. The less similar neighbor cells are to each other, the higher the value of abs$[1 - S_n/S_{n-1}]$. Note both *ICD* and *dICD* cells have an intermediate phenotype that is not significantly different from either control or *shFatl9*; differences between control and *shFatl9* are significant (***$P = 0.0003$) and not significant between control and *FoxO* ($P = 0.3235$); mean with SD, two-tailed *t* test. In *I* and *J* data collected from three animals of *FoxO* and four to six animals of each of the other lines. (*K*) Circularity of the control and *shFatl9* knockdown cells. Mean with SD, two-tailed *t* test, ***$P < 0.0001$; data were collected from six control animals and three of each *shFatl9* and *FoxO*.

detected on the apical surface of ectodermal epithelial cells; however, in overexpression conditions, ICD-GFP and dICD-GFP are found at apical membranes (Fig. 4*G*), where it can induce microvilli. Similarly, ectopic expression of the intracellular domain of MmFat1 can induce actin polymerization at ectopic sites (6). In contrast, overexpression of HyFatl ICD did not alter the amount of actin at adherens junctions, as assessed by phalloidin staining, suggesting that HyFatl may have spatially restricted effects on the cytoskeleton.

Interestingly, planar polarization of *Hydra* Ds occurs without the presence of a classical Fat cadherin. This indicates that Ds homologs can function independently of Fat/Fat4 cadherins in *Hydra*. Although Fat and Ds cadherins often function together, work in *Drosophila* and zebrafish has suggested that Ds cadherins may have Fat-independent functions (45–47). In addition, interactions between Ds and Fat-like cadherins have not been reported in other organisms. We cannot exclude the possibility that HyDs and HyFatl interact; however, ectopic expression of HyFatl ICD does not change the polarization of HyDs.

All of the proteins making up the core PCP module in bilaterians have been found in anthozoan and medusozoan cnidarians (11, 15) as well as in *Trichoplax* and some sponge species (11). This suggests the basic PCP machinery was established before the appearance of bilaterians. Cadherin molecules designated as Fat homologs have been identified in lineages that diverged prior to Cnidaria (9, 24). However, the molecular structure of these putative Fat proteins, in particular the number of cadherin repeats, varies dramatically: 14 in *Amphimedon queenslandica*, 37 in *Monosiga brevicollis*, and 9 in *Trichoplax adhaerens*. In contrast, the anthozoan cnidarian *Nematostella* has a complete repertoire of atypical cadherins involved in PCP with a clear Fat homolog (24). *Hydra* and other medusozoan cnidarians have only a single Fat-like cadherin, but lack a true Fat homolog, which may have been lost during evolution. Thus, the anthozoans are the only nonbilaterian with a Fat homolog. Interestingly, anthozoans are distinct from other cnidarians in having bilaterality displayed by a pair of directive mesenteries and an asymmetric siphonoglyph (reviewed in ref. 48). It is interesting to speculate that the addition of a Fat/Ds module to the

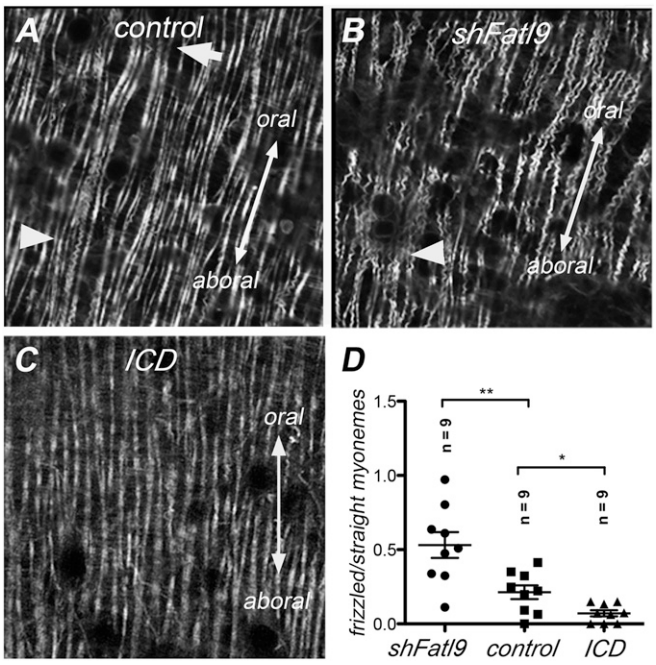

Fig. 8. Actin cables in ectodermal myonemes change morphology upon down-regulation of *HyFatl*. (*A–C*) Actin in ectodermal myonemes was visualized with phalloidin; arrow points to the straight and arrowheads to the "frizzled" myonemes. (*D*) Graph showing the ratio of frizzled and straight actin fibers measured for n number of confocal images, 50 to 90 myonemes per image. Mean with SD, two-tailed *t* test, $*P = 0.0133$, $**P = 0.0052$, five to six animals of each line.

core complex could have led to a new level of planar cell polarization and appearance of a second axis of symmetry. This intriguing scenario calls for functional studies of *Fat* and *Ds* in anthozoans, e.g., *Nematostella*.

In summary, our studies indicate that planar polarization of Fat-like and Ds cadherins was established before the divergence of cnidarians and bilaterians, and that Fat-like cadherins have roles in tissue organization, cell adhesion, and the cytoskeleton in *Hydra*.

Materials and Methods

See *SI Appendix* for the full description of *Materials and Methods*.

Animals, Culture Conditions, and Transplantation Experiments. The AEP strain of *Hydra vulgaris* was cultured at 18 °C in hydra medium (1.0 mM $CaCl_2$, 1 mM $NaHCO_3$, 0.1 mM $MgCl_2$, 0.03 mM KNO_3, 1 mM Tris HCl, pH 7.8, and fed with *Artemia nauplii* every 2 d.

In Situ Hybridization. Briefly: samples were fixed in 4% paraformaldehyde (PFA) and hybridized with antisense dioxygenin-labeled RNA probe at 0.1 ng/μL; after removal of the probe, samples were incubated with alkaline phosphatase-conjugated anti-digoxygenin Fab fragments; alkaline phosphatase reaction was carried out at 37 °C in the presence of 5 μL/mL nitro-blue tetrazolium chloride (NBT) and 3.75 μL/mL 5-Bromo-4-chloro-3-indolyl phosphate (BCIP) in the dark.

Production of Antibodies. Peptides corresponding to the C-terminal portions of HyFat (residues 4,191 to 4,393) and HyDs (residues 9,144 to 9,799) were expressed as GST fusions using the GEX4t-1 vector (Millipore) in *Escherichia coli* strain BL21 and purified on glutathione-agarose (Thermo Scientific). Purified proteins were used to immunize guinea pigs (Cocalico Biologicals) and rats (Covance). Polyclonal antibodies were purified by binding to antigen immobilized on glutathione-agarose beads and elution with 100 mM glycine (pH 2.5) into 1 M Tris, pH 8.0.

Immunoblot and Immunofluorescence Analysis. To perform immunocytochemistry on whole mounts, animals were relaxed in 2% urethane for 2 min, and then fixed in either Lavdovski's fixative (ethanol:formaldehyde:acetic acid:H_2O 50:10:4:36) for HyFatl, HyDs, GFP, phospho-Histone H3, and FGF2 antibodies, or in 4% paraformaldehyde for phalloidin staining overnight at 4 °C. Primary antibody dilutions were as follows: anti-HyFat total serum, 1:1,000; affinity-purified anti-HyFat, 1:100; anti-HyDs total serum, 1:400; affinity-purified anti-HyDs, 1:100; anti-GFP (Abcam, ab13970), 1:400; anti-phospho Histone H3 (Millipore, 05-806), 1:400; anti-FGF2 (Santi Cruz, sc7911), 1:100. Fluor-conjugated secondary antibodies (The Jackson Laboratory) were used at 1:400 dilution. Alexa555-phalloidin (Abcam) was used at 1:1,000 dilution.

Database Search and Phylogenetic Analysis. To identify cnidarian homologs of Fat-like, Ds, and CELSR proteins we searched the NCBI (https://www.ncbi.nlm.nih.gov/) and National Human Genome Research Institute (NHGRI) (https://research.nhgri.nih.gov) databases. As queries, we have used sequences of the intracellular portions of *N. vectensis* Fat-like, Ds, and CELSR proteins (10). We have identified *H. vulgaris* homologs of Fat-like (XM_012702814.1, former XM_002167158.2), Ds (PT_comp25284_c0_seq1), and CELSR (XM_002163205), *Alatina alata* partial sequences of Fat-like (GEUJ01029859.1) and Ds (GEUJ01029600.1) homologs, *Cassiopea xamachana* partial sequences of Fat-like (OLMO01020275.1) and Ds (OLMO01079121.1), *Aurelia aurita* Fat-like homolog (GHAI01167428.1), and *Hydractinia symbiolongicarpus* partial Fat-like sequence (GAWH01043253.1). For generation of the phylogenetic tree, the sequences were aligned using MAFFT (https://www.ebi.ac.uk/Tools/msa/mafft/).

Data Availability.

All data are contained in the manuscript text and *SI Appendix*.

ACKNOWLEDGMENTS. We are grateful to Bert Hobmayer (University of Innsbruck) for providing the *claudin-GFP* transgenic *Hydra* and the AEP strain of *H. vulgaris*; Jörg Wittlieb (University of Kiel) for generating transgenic lines; Celina Juliano (University of California, Davis) and Hiroshi Shimizu (King Abdullah University of Science and Technology) for providing the AEP *H. vulgaris* strain; Dae-Kyum Kim (Lunenfeld-Tanenbaum Research Institute) for helping with the statistical analysis; and Brigitte Galliot (University of Geneva) for providing the FGF2 antibody. We thank anonymous reviewers for their critique and constructive suggestions. M. Brooun and H.M. were funded by the Natural Sciences and Engineering Research Council of Canada grant RGPIN-2016-06354. H.M. was supported by a Canadian Institutes of Health Research foundation grant (FDN 143319) and start up funds from Washington University School of Medicine. B.J.P. was supported by Ontario Institute for Cancer Research grant IA-026.

1. D. Devenport, The cell biology of planar cell polarity. *J. Cell Biol.* **207**, 171–179 (2014).
2. A. D. Fulford, H. McNeill, Fat/Dachsous family cadherins in cell and tissue organisation. *Curr. Opin. Cell Biol.* **62**, 96–103 (2020).
3. P. Sharma, H. McNeill, Fat and Dachsous cadherins. *Prog. Mol. Biol. Transl. Sci.* **116**, 215–235 (2013).
4. D. Y. Chen, K. R. Lipari, Y. Dehghan, S. J. Streichan, D. Bilder, Symmetry breaking in an edgeless epithelium by fat2-regulated microtubule polarity. *Cell Rep.* **15**, 1125–1133 (2016).
5. S. Matsui *et al.*, Knockdown of Fat2 by siRNA inhibits the migration of human squamous carcinoma cells. *J. Dermatol. Sci.* **51**, 207–210 (2008).
6. M. J. Moeller *et al.*, Protocadherin FAT1 binds Ena/VASP proteins and is necessary for actin dynamics and cell polarization. *EMBO J.* **23**, 3769–3779 (2004).
7. A. J. Squarr *et al.*, Fat2 acts through the WAVE regulatory complex to drive collective cell migration during tissue rotation. *J. Cell Biol.* **212**, 591–603 (2016).
8. T. Tanoue, M. Takeichi, Mammalian Fat1 cadherin regulates actin dynamics and cell-cell contact. *J. Cell Biol.* **165**, 517–528 (2004).
9. M. Abedin, N. King, The premetazoan ancestry of cadherins. *Science* **319**, 946–948 (2008).
10. P. Hulpiau, F. van Roy, Molecular evolution of the cadherin superfamily. *Int. J. Biochem. Cell Biol.* **41**, 349–369 (2009).
11. Q. Schenkelaars, L. Fierro-Constain, E. Renard, C. Borchiellini, Retracing the path of planar cell polarity. *BMC Evol. Biol.* **16**, 69 (2016).
12. A. Sebé-Pedrós, Y. Zheng, I. Ruiz-Trillo, D. Pan, Premetazoan origin of the hippo signaling pathway. *Cell Rep.* **1**, 13–20 (2012).
13. T. Momose, Y. Kraus, E. Houliston, A conserved function for Strabismus in establishing planar cell polarity in the ciliated ectoderm during cnidarian larval development. *Development* **139**, 4374–4382 (2012).
14. S. Kumburegama, N. Wijesena, R. Xu, A. H. Wikramanayake, Strabismus-mediated primary archenteron invagination is uncoupled from Wnt/β-catenin-dependent endoderm cell fate specification in Nematostella vectensis (Anthozoa, Cnidaria): Implications for the evolution of gastrulation. *Evodevo* **2**, 2 (2011).
15. I. Philipp *et al.*, Wnt/beta-catenin and noncanonical Wnt signaling interact in tissue evagination in the simple eumetazoan Hydra. *Proc. Natl. Acad. Sci. U.S.A.* **106**, 4290–4295 (2009).

16. H. R. Bode, The interstitial cell lineage of hydra: A stem cell system that arose early in evolution. *J. Cell Sci.* **109**, 1155–1164 (1996).
17. R. D. Campbell, Tissue dynamics of steady state growth in Hydra littoralis. II. Patterns of tissue movement. *J. Morphol.* **121**, 19–28 (1967).
18. H. Shimizu, P. M. Bode, H. R. Bode, Patterns of oriented cell division during the steady-state morphogenesis of the body column in hydra. *Dev. Dyn.* **204**, 349–357 (1995).
19. H. R. Bode, Axial patterning in hydra. *Cold Spring Harb. Perspect. Biol.* **1**, a000463 (2009).
20. K. Niebuhr *et al*., A novel proline-rich motif present in ActA of Listeria monocytogenes and cytoskeletal proteins is the ligand for the EVH1 domain, a protein module present in the Ena/VASP family. *EMBO J.* **16**, 5433–5444 (1997).
21. H. Cheng, J. Burroughs-Garcia, J. E. Birkness, J. C. Trinidad, M. R. Deans, Disparate regulatory mechanisms control Fat3 and P75NTR protein transport through a conserved kif5-interaction domain. *PLoS One* **11**, e0165519 (2016).
22. H. F. Clark *et al*., Dachsous encodes a member of the cadherin superfamily that controls imaginal disc morphogenesis in Drosophila. *Genes Dev.* **9**, 1530–1542 (1995).
23. D. N. Clarke, P. W. Miller, C. J. Lowe, W. I. Weis, W. J. Nelson, Characterization of the cadherin-catenin complex of the sea anemone Nematostella vectensis and implications for the evolution of metazoan cell-cell adhesion. *Mol. Biol. Evol.* **33**, 2016–2029 (2016).
24. P. Hulpiau, F. van Roy, New insights into the evolution of metazoan cadherins. *Mol. Biol. Evol.* **28**, 647–657 (2011).
25. T. Usui *et al*., Flamingo, a seven-pass transmembrane cadherin, regulates planar cell polarity under the control of Frizzled. *Cell* **98**, 585–595 (1999).
26. Y. Feng, K. D. Irvine, Processing and phosphorylation of the Fat receptor. *Proc. Natl. Acad. Sci. U.S.A.* **106**, 11989–11994 (2009).
27. E. Sadeqzadeh *et al*., Dual processing of FAT1 cadherin protein by human melanoma cells generates distinct protein products. *J. Biol. Chem.* **286**, 28181–28191 (2011).
28. A. Sing *et al*., The atypical cadherin fat directly regulates mitochondrial function and metabolic state. *Cell* **158**, 1293–1308 (2014).
29. R. Sopko *et al*., Phosphorylation of the tumor suppressor fat is regulated by its ligand Dachsous and the kinase discs overgrown. *Curr. Biol.* **19**, 1112–1117 (2009).
30. K. Barlan, M. Cetera, S. Horne-Badovinac, Fat2 and lar define a basally localized planar signaling system controlling collective cell migration. *Dev. Cell* **40**, 467–477.e5 (2017).
31. I. Viktorinová, T. König, K. Schlichting, C. Dahmann, The cadherin Fat2 is required for planar cell polarity in the Drosophila ovary. *Development* **136**, 4123–4132 (2009).
32. W. Buzgariu, S. Al Haddad, S. Tomczyk, Y. Wenger, B. Galliot, Multi-functionality and plasticity characterize epithelial cells in Hydra. *Tissue Barriers* **3**, e1068908 (2015).
33. A. Krol, S. J. Henle, L. V. Goodrich, Fat3 and Ena/VASP proteins influence the emergence of asymmetric cell morphology in the developing retina. *Development* **143**, 2172–2182 (2016).
34. J. J. Otto, R. D. Campbell, Budding in Hydra attenuata: Bud stages and fate map. *J. Exp. Zool.* **200**, 417–428 (1977).
35. R. Aufschnaiter, R. Wedlich-Söldner, X. Zhang, B. Hobmayer, Apical and basal epitheliomuscular F-actin dynamics during *Hydra* bud evagination. *Biol. Open* **6**, 1137–1148 (2017).
36. T. W. Holstein, E. Hobmayer, C. N. David, Pattern of epithelial cell cycling in hydra. *Dev. Biol.* **148**, 602–611 (1991).
37. J. J. Otto, R. D. Campbell, Tissue economics of hydra: Regulation of cell cycle, animal size and development by controlled feeding rates. *J. Cell Sci.* **28**, 117–132 (1977).
38. U. Technau *et al*., Parameters of self-organization in Hydra aggregates. *Proc. Natl. Acad. Sci. U.S.A.* **97**, 12127–12131 (2000).
39. J. Wittlieb, K. Khalturin, J. U. Lohmann, F. Anton-Erxleben, T. C. Bosch, Transgenic Hydra allow in vivo tracking of individual stem cells during morphogenesis. *Proc. Natl. Acad. Sci. U.S.A.* **103**, 6208–6211 (2006).
40. A. M. Boehm *et al*., FoxO is a critical regulator of stem cell maintenance in immortal Hydra. *Proc. Natl. Acad. Sci. U.S.A.* **109**, 19697–19702 (2012).
41. A. Klimovich *et al*., Non-senescent *Hydra* tolerates severe disturbances in the nuclear lamina. *Aging (Albany NY)* **10**, 951–972 (2018).
42. D. L. West, The epitheliomuscular cell of hydra: Its fine structure, three-dimensional architecture and relation to morphogenesis. *Tissue Cell* **10**, 629–646 (1978).
43. S. Blair, H. McNeill, Big roles for Fat cadherins. *Curr. Opin. Cell Biol.* **51**, 73–80 (2018).
44. F. Aurich, C. Dahmann, A mutation in fat2 uncouples tissue elongation from global tissue rotation. *Cell Rep.* **14**, 2503–2510 (2016).
45. J. Chen *et al*., Atypical cadherin Dachsous1b interacts with Ttc28 and aurora B to control microtubule dynamics in embryonic cleavages. *Dev. Cell* **45**, 376–391.e5 (2018).
46. J. L. Degoutin *et al*., Riquiqui and minibrain are regulators of the hippo pathway downstream of Dachsous. *Nat. Cell Biol.* **15**, 1176–1185 (2013).
47. M. Willecke, F. Hamaratoglu, L. Sansores-Garcia, C. Tao, G. Halder, Boundaries of Dachsous Cadherin activity modulate the Hippo signaling pathway to induce cell proliferation. *Proc. Natl. Acad. Sci. U.S.A.* **105**, 14897–14902 (2008).
48. S. Berking, Generation of bilateral symmetry in anthozoa: A model. *J. Theor. Biol.* **246**, 477–490 (2007).